Journal of Membrane Science 610 (2020) 118292

Contents lists available at ScienceDirect

Journal of Membrane Science

journal homepage: http://www.elsevier.com/locate/memsci

Modelling temperature effects in a membrane cascade system for oligosaccharides

Zulhaj Rizki [a,*], Eric Suryawirawan [a], Anja E.M. Janssen [a], Albert van der Padt [a,b], Remko M. Boom [a]

[a] Wageningen University, Food Process Engineering Group, PO Box 17, 6700 AA, Wageningen, the Netherlands
[b] FrieslandCampina, Stationsplein 4, Amersfoort, 3818 LE, the Netherlands

ARTICLE INFO

Keywords:
Temperature effect
Membrane cascades
Oligosaccharide fractionation
Modelling
Nanofiltration

ABSTRACT

Open nanofiltration of mixtures of fructo-oligosaccharides was assessed by experiment and by modelling the overall permeation behaviour of 3 different membranes. The temperature effect was modelled using the steric pore model, incorporating the molecular volumetric expansion of fructo-oligosaccharides as solutes, the decrease in the solution viscosity and the volumetric expansion of the membrane with increasing temperature. The thermal expansion of the solute was described as a linear increase in the bare molecular volume plus a non-linear decrease in its hydration number. The viscosity reduction was modelled by incorporating the temperature as a variable into an existing exponential relation derived by Chirife and Buera. The thermal expansion of membranes was described with a linear increase in the pore size and a linear decrease in its hydrodynamic resistance. Although the purity of the oligosaccharide product was hardly affected by the temperature, the yield was much lower at higher temperatures. The yield can therefore be improved by decreasing the temperature while maintaining the product purity. This behaviour was also observed in a 3-stage filtration cascade. The temperature effect is closely related to the increase in fluxes with temperature, leading to a different split of the feed into permeate and retentate. In a membrane cascade, the lower yield with higher temperatures was seen most strongly at the top stage, and much less at the middle and lower stages, which can be explained by the configuration of the cascade.

1. Introduction

Membrane separation has become popular to fractionate food components, due to its simplicity, mild operating conditions and relative cost effectiveness compared with other separation processes. Its implementation varies from ultrafiltration for protein separation [1] and nanofiltration for separation of sugars and carbohydrates [2–5] to reverse osmosis for removing salts [6]. Each application needs a particular membrane and an appropriate process design for optimum performance. Designing a membrane process can be time consuming, but a proper model aids the designer to determine which process parameters should be applied and which properties of the membrane are required [7–9].

Here, we concentrate on the interface of nanofiltration and ultrafiltration, open nanofiltration, for the fractionation of oligosaccharides. The Donnan Steric Pore Model (DSPM) has been used extensively for this. This approach combines the diffusive, convective and electrical transport inside the membrane [10]. Apart from the electrical interactions, this model also explains the sieving mechanism for neutral solutes [11,12]. Coupled with a mass transfer model that describes the transport phenomena outside the membrane, this DSPM model has been modified and applied to various applications [13–16].

Oligosaccharide fractionation has become an important application for membrane separation. Some oligosaccharides have prebiotic properties [17–20] and improve the rheological behaviour [21–23] of food products; however, mono- and disaccharides are sweet and increase the caloric density of a product. Oligosaccharide fractionation with membrane processes has been explored using an experimental approach [4,24] that was then extended to models [3,25,26]. Multistage membrane processes have also been investigated to improve the fractionation of oligosaccharides, both as a consecutive configuration without recycle [24,27] and as a cascaded configuration with recycle [28–30].

Most experiments and models have been explored using specific operating conditions, typically at one particular operating temperature.

* Corresponding author.
E-mail address: zulhaj.zulhajrizki@wur.nl (Z. Rizki).

https://doi.org/10.1016/j.memsci.2020.118292
Received 2 March 2020; Received in revised form 18 May 2020; Accepted 20 May 2020
Available online 26 May 2020

The operating temperature is known to have a strong effect, for example, on the transmembrane fluxes and is believed to have an effect on other aspects as well [16,31,32]. However, it has not yet been explicitly included in the models. A change in temperature often requires reformulating the models or carrying out more experiments to determine the values of the parameters at the new temperature. Therefore, it is important to develop a model that explicitly considers the effect of temperature as a process variable.

In cascades of membranes, it is possible to use different conditions at each stage to achieve better overall performance [29,30,33,34]. So far, inhomogeneous cascades have been operated using the same temperature at each stage while various membranes and pressure were used; however, we foresee that a cascade that operates at different temperatures in each stage may perform better.

In this paper, we develop an integrated model that includes the influence of the temperature in the nanofiltration of oligosaccharides for a single-stage membrane. This model is expanded later towards a cascade system to explore the benefit of having different temperatures in the cascade setup.

2. Model development

We use the steric pore model (SPM, which is a simplification of the DSPM, valid for neutral solutes) for the transport inside the membrane. According to this model, the separation mechanism for a neutral solute is pure sieving via convective and diffusive transfer. In this model, the molecular dimensions of solutes and the membrane pore size determine the separation as well as the solution properties, such as the viscosity and the solute diffusivities. By combining this theory with an appropriate concentration polarization model, we can predict the overall performance of the membrane.

2.1. Temperature effect on the molecular volume of fructo-oligosaccharides

Most derivatives of the SPM consider the solutes to be spherical. The dimension of these solutes is characterized using the Stokes radius ($r_{S,\,i}$), which can be estimated from its diffusivity (equation (1)). This diffusivity can be estimated using a relation derived by Sano and Yamamoto [35] that depends on its molecular weight (equation (2)).

$$r_{S,\,i} = \frac{k_B \;\; T}{6 \;\; \pi \;\; D_i} \tag{1}$$

$$D_i = \frac{T}{9.5 \;\; \times \;\; 10^{13} \;\; MW^{1/3} \;\; \eta} \tag{2}$$

Fructo-oligosaccharides (FOS) are oligomers of fructose with glucose; they have a chain-like structure and are therefore definitely not spherical. This is typically not considered in most models. Recently, Aguirre et al. [14] modelled the filtration of FOS by considering them as elongated capsules with 2 dimensions: diameter ($L_{0,\,i}$) and length ($L_{1,\,i}$). They compared 3 ways to include these dimensions: (1) considering them as completely spherical using their Stokes radii, (2) considering them as completely capsular using both the capsule diameter and length, and (3) using a semi-capsular approach with the so-called Giddings radius [36] as an average of both the capsule radius and the half-capsule length (equation (3)). Both the complete capsular and the semi-capsular approaches predicted the filtration performance better than the spherical approach. Since the full capsular model is complex and requires significant computation time, the semi-capsular approach was adopted for further use. In this approach, each oligosaccharide is characterized by its own diameter and length, and then its Giddings radius, $r_{G,i}$, is used for further calculations.

$$r_{G,i}(T) = \frac{1}{4}(L_{0,\,i}(T) + \;\; L_{1,\,i}(T)) \tag{3}$$

The FOS capsules are constructed using spheres of hydrated glucose and fructose as building blocks (Fig. 1). The capsule half-length is estimated from the sum of the radius of each sphere. The sphere radius is calculated using the hydrated molar volume and assuming the monosaccharide to be a perfect sphere. Unlike glucose, the dimension of a hydrated fructose in a chain may differ from its free form. To construct the FOS capsules, the dimension of hydrated fructose in a chain is used, which is estimated by subtracting the molar volume of glucose from that of sucrose.

In general, the molar volume of hydrated sugars, $V_{m,h}$, can be expressed as the total volume of the non-hydrated sugar, $V_{m,b}$, plus the water that is bound to it. The amount of bound water can be estimated by the hydration number of a particular sugar, n_h, multiplied by the volume of the individual bound water molecules, $V_{m,bw}$.

$$V_{m,\mathrm{h}}(T) = V_{m,b} \;\; (T) + V_{m,bw} n_h(T) \tag{4}$$

The parameters in equation (4) were investigated by Gharsallaoui et al. [37] using sugar density data. They proposed different values for the non-hydrated volumes, bound water volumes and hydration numbers for mono- and disaccharides at several chosen temperatures. However, they did not propose a clear relation between the temperature and these parameters.

Gharsallaoui et al. [37] proposed values for the individual bound water volume between 16.4 and 17.2 mL/mol for sucrose in a

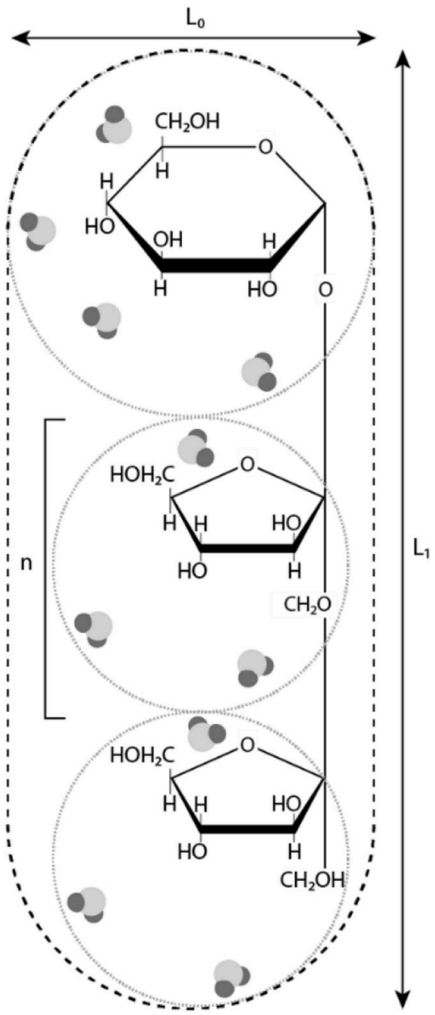

Fig. 1. Graphical representation of a FOS capsule. The capsule is composed of spherical hydrated monosaccharides as its building blocks. The capsule is characterized by the capsule diameter L_0 and capsule length, L_1. Adapted from Aguirre et al. [14].

temperature range of 0 °C–100 °C, and 16.2 mL/mol for glucose at 20 °C. The bound water volume is somewhat dependent on the type of sugars it binds to as a monomer, and its dependence on temperature is not clear. Therefore, we used a constant value of 16.5 mL/mol for the bound water volume of both sucrose and glucose, which we can assume to be accurate in between 25 °C and 45 °C.

Using density data, Gharsalloui et al. [37] then estimated the molar volume of non-hydrated sucrose, $V_{m,b}$, at several temperature points between 20 °C and 80 °C. Those estimates showed a linear relationship with the temperature (equation (5)). Unlike sucrose, the data for glucose density at various temperature is not widely available. However, it is possible to estimate the molar volume of non-hydrated glucose with the partial molar volume of glucose at infinite dilution, as was derived by Fucaloro et al. [38]. Both approaches gave more or less the same estimates for the molar volume of sucrose at 20 °C. Therefore, we can use Fucaloro et al.'s data for the temperature dependency of $V_{m,b}$ for glucose as well. As found with sucrose, the molar volume of non-hydrated glucose is also linear with the temperature (equation (6)). Both molar volumes in equations (5) and (6) are presented in mL/mol and temperatures in °C (Fig. 2).

$$V_{m,b}(T)_{sucrose} = 219.55 + 0.07T \tag{5}$$

$$V_{m,b}(T)_{glucose} = 109.41 + 0.09T \tag{6}$$

The hydration numbers of both sucrose and glucose are not linear with the temperature. Gharsalloui et al. [37] fitted a quadratic equation to the hydration number of sucrose and temperature (in °C), as shown in equation (7). A similar approach can be taken for glucose using the data from Shiio [39]; a quadratic relationship (equation (8)) was also found here. The hydration number is plotted versus the temperature in Fig. 3.

$$n_H(T)_{sucrose} = 7.1 - 0.06\ \ T + 3.69\ \ \times 10^{-4}\ \ T^2 \tag{7}$$

$$n_H(T)_{glucose} = 7.22 - 0.19\ \ T + 1.70\ \ \times 10^{-3}\ \ T^2 \tag{8}$$

The combination of the molar volumes of the unhydrated molecules and the hydration numbers of sucrose and glucose enables us to estimate their hydrated molar volumes and with that, the dimension of FOS with any degree of polymerization (DP). At a given temperature, the molar volume of glucose and sucrose can be estimated using equations (4)–(8). With these values, we can calculate the molar volume of fructose in a chain. Assuming that the hydrated monosaccharides have a spherical shape, the length, $L_{0,\,i}$, of the glucose and fructose monomers in the chain can be calculated. Assuming that all FOS chains have only one glucose monomer (see Fig. 1), the capsule length of FOS at a certain DP can be estimated using equation (9). The capsule diameter is equal to the largest diameter of the monomers, glucose.

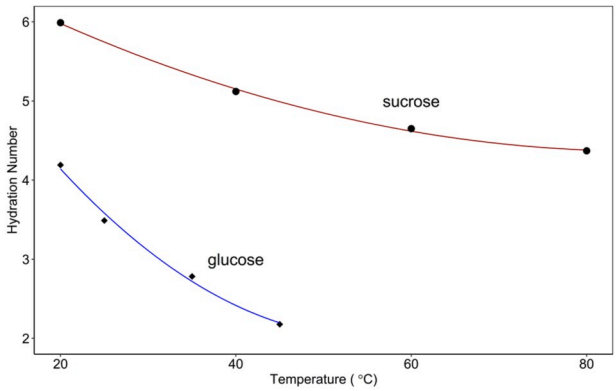

Fig. 3. Quadratic fitting of the hydration number as a function of temperature for sucrose based on the work of Gharsallaoui et al. [37] and glucose based on the work of Shiio [39].

$$L_{1,\,i} = L_{0,\,glucose} + (DP_i - 1)\ \ L_{0,\,fructose} \tag{9}$$

2.2. Temperature effect on viscosity

Chirife and Buera [40] have derived a model to predict the viscosity of sugar mixtures, η_s with an exponential relation to sugar concentration relative to the viscosity of water, η_w, (equation (10)).

$$\frac{\eta_s}{\eta_w} = a\ \ \exp(EX) \tag{10}$$

Both a and E are fitting parameters. To predict the sugar viscosity, these parameters need to be estimated. In most cases, a is close to unity.

The value of E differs for every mixture and shows a linear relationship with the average molecular weight (equation (11)).

$$E = b\overline{MW} + c \tag{11}$$

Using equation (12), the viscosities of any sugar solutions with known average molecular weight can be estimated. This is not limited to simple sugars, because this model has been validated for

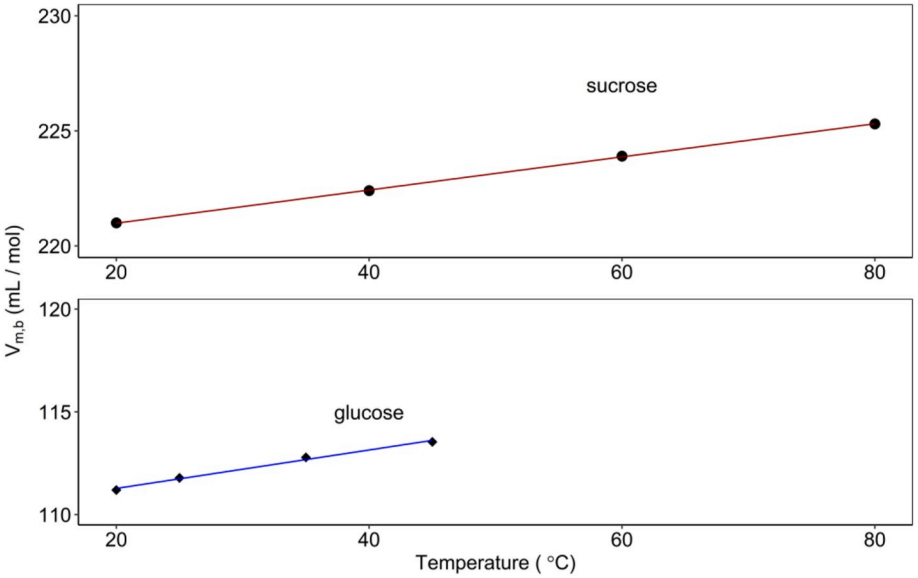

Fig. 2. Linear relationship between the temperature and bare volume of sucrose derived from density data [37] and fructose derived from infinite dilution [38].

oligosaccharides by knowing their average molecular weight.

Aguirre et al. [29] and Rizki et al. [30] reported estimates of the parameters in equations (10) and (11) for FOS at 45 °C. To use these equations for other operating temperatures, we need to either estimate the parameters at each temperature point or define the temperature dependency of these estimates. Chirife et al. [41] reported a temperature dependency of E as in equation (12),

$$E = \frac{\Delta G}{R_g T} \tag{12}$$

in which ΔG represents the free energy of activation for viscous flow per mole of solute. Combining this with equations (10) and (11) yields equation (13).

$$\frac{\eta_s}{\eta_w} = a \exp\left[\left(\frac{b^* \overline{MW} + c^*}{R_g T}\right) X\right] \tag{13}$$

In this equation, parameters b^* and c^* represent the activation energy and its dependency on molecular weight. Therefore, this modified equation is applicable for mixtures with any average molecular weight and different operating temperatures.

2.3. Mass transfer model

In the absence of a cake or fouling layer on the membrane, the volumetric flux, J_v, can be calculated using Darcy's law and the effective pressure difference across the membrane, the solution viscosity and the membrane resistance, R_m. The effective pressure is defined as the transmembrane pressure, *TMP*, corrected for the osmotic pressure difference across the membrane that results from the concentration gradient between 2 sides of the membrane after considering the extent of the polarization concentration (equation (14)). The osmotic pressure can be estimated using Van't Hoff's equation (equation (15)).

$$J_v = \frac{TMP - \Delta\pi_o}{\eta R_m} \tag{14}$$

$$\Delta\pi_o = \sum_{i=1}^{n} (C_{m,i} - C_{p,i}) R_g T \tag{15}$$

The concentration at the membrane surface, $C_{m,i}$, has a higher value than that in the bulk as a consequence of concentration polarization, which can be calculated once we know the mass transfer coefficient, k_i. We can estimate the mass transfer coefficient, k_i, using a Sherwood relation. For spiral wound modules, the relationship proposed by Schock and Miquel [42] is widely used. In addition to k_i, Stewart [43] proposed a correction on the mass transfer coefficient that corrects for flow stabilizing effects due to the suction of the solvent into the membrane (equation (16)). Some models neglect this correction, which is presumably acceptable for low fluxes. At low flux, the corrected mass transfer coefficient is close to its original estimate, whereas its value deviates more at higher flux.

$$\frac{k_i^*}{k_i} = \frac{J_v/k_i}{[1 - exp(-J_v/k_i)]} \tag{16}$$

Recently, Aguirre et al. [14] applied a modified SPM to the transport of FOS inside a membrane based on the work of Bowen and Welfoot [44,45]. In their approach, the solute flux of a neutral component is expressed as the sum of convective and diffusive transport resulting from the concentration and pressure gradients across the membrane (equation (17)). In equation (17), C_i represents the local concentration as a function of the axial position, z.

$$J_i = K_{c,i} C_i V - D_{p,i} \frac{dC_i}{dz} - \frac{C_i D_{p,i}}{R_g T} V_m \frac{dP}{dz} \tag{17}$$

The convective part of the flux equation depends on the local concentration C_i, the solvent velocity inside the pore V, and a convective hindrance coefficient $K_{c,i}$. Assuming a cylindrical pore, the average solvent velocity may be approached using the Hagen-Poisseuille equation (equation (18)). This equation was developed for a single cylinder. Assuming the membrane consists of parallel pores, this relation is also valid for a porous membrane. The porosity itself is considered in the effective membrane surface.

The hindrance coefficient for a solute through a cylinder can be expressed as a function of the ratio of the solute size to the pore width, λ_i, referring to the work of Dechadilok and Deen [46]. This relation was adapted by Aguirre et al. [14] by substituting the solute radius with the average Giddings radius (equation (19)).

$$V = -\frac{r_p^2 \Delta P}{8 \eta \Delta x} \tag{18}$$

$$K_{c,i} = \frac{1 + 3.867 \lambda_i - 1.907 \lambda_i^2 - 0.834 \lambda_i^3}{1 + 1.867 \lambda_i - 0.741 \lambda_i^2} \quad \text{with} \quad \lambda_i = \frac{r_{G,i}}{r_p} \tag{19}$$

Inside the pore, the diffusivity of a solute $D_{p,i}$, is corrected with a hindrance coefficient, K_d, and a relative viscosity increase, η_r (equation (21)). This increase in viscosity is explained by many authors as a consequence of a thin, stagnant water layer that is attached to the pore wall, leaving less volume for diffusion of a solute. In this equation, d_w represents the thickness of this stagnant water layer, which is estimated to be 0.28 nm, the typical size of a water molecule.

$$D_{p,i} = \frac{K_d D_i}{\eta_r} \tag{20}$$

$$\eta_r = 1 + 18\frac{d_w}{r_p} - 9\left(\frac{d_w}{r_p}\right)^2 \tag{21}$$

$$K_d = \frac{9}{4}\pi^2\sqrt{2}(1-\lambda)^{-5/2}\left[1 - \frac{73}{60}(1-\lambda) + \frac{77293}{50400}(1-\lambda)^2 - 22.5083 - 5.6117\lambda - 0.3363\lambda^2 - 1.216\lambda^3 + 1.647\lambda^4\right] \tag{22}$$

Solving equation (17) with boundary conditions, $C_i = \varphi_i C_{m,i}$ at $z = 0$ and $C_i = \varphi_i C_{p,i}$ at $z = \Delta z$, allows us to predict the solute real rejection coefficient, $R_{r,i}$ (equation (23)). The real rejection coefficient relates to the solute concentration at the membrane surface, which is estimated by taking into account the concentration polarization phenomenon (equation (26)). The partition coefficient, φ_i, is estimated as a function of the solute to pore ratio, λ_i, following the work of Dechadilok and Deen [46] for a cylindrical pore.

$$R_{r,i} = 1 - \frac{(K_{c,i} - K_{Y,i})\varphi_i}{1 - [1 - (K_c - K_Y)\varphi_i] exp(-Pe)} \tag{23}$$

$$Pe = -\frac{(K_{c,i} - K_{Y,i}) r_p^2}{8\eta D_{p,i}} \Delta P \tag{24}$$

$$K_Y = -\frac{D_{p,i}}{R_g T} V_m \frac{8\eta}{r_p^2} \quad (25)$$

$$R_{r,i} = 1 - \frac{C_{p,i}}{C_{m,i}} \quad (26)$$

$$\varphi_i = 1 - \lambda_i^2 \quad (27)$$

2.4. Pore size distribution

In the model described in Section 2.3, the solute rejection is dependent only on the size of the individual pore. However, estimating the pore size by fitting the experimental rejection with the SPM for a mixture of FOS results in a different estimated pore size for each oligosaccharide. This is somewhat overlooked in the literature, because most publications using the SPM report on studies for single solutes. However, it is very important when dealing with mixtures.

The different pore sizes obtained with different solutes can be explained by the pore size distribution in the membrane. Even though the SPM can predict the rejection of a single cylindrical pore, not all pores are equally accessible to all solutes; larger solutes may not enter a smaller pore at all. All practical membranes have pore size distributions.

Bowen and Welfoot [44] incorporated the pore size distribution into the SPM, but only for a single solute. Based on their work, Aguirre et al. [14] predicted the rejection of FOS for a mixture by expanding equation (23) to all pores in the membrane, assuming a normal distribution. As a consequence, the membrane is characterized by 2 intrinsic parameters: the average pore size and the standard deviation in the pore size. This has the drawback that estimating 2 parameters in a complex, non-linear model is not trivial.

Another approach to incorporate a pore size distribution related to multicomponent mixture permeation was proposed by Kuhn et al. [3]. They assumed that some pores retain some solutes, whereas other pores let these pass freely, which they called non-rejecting pores. Further, they calculated the ratio between the flux via the non-rejecting pores for each solute and the pure water flux, i.e. the solvent flux through all pores. A pore size distribution can be derived by differentiating this ratio to the pore size fitted from the SPM. In this way, a mean pore size and a standard deviation can be estimated, assuming a normal distribution of pore sizes. This yields the 2 similar parameters as in Aguirre et al.'s [14] approach.

2.5. Temperature effect on membrane properties

The expansion of a material is in general relatively linear over the temperature interval of interest here. If the membrane expands with temperature, it is logical that the membrane pores expand at the same rate. Therefore, we can describe the temperature effect on the membrane pore size using a one-dimensional thermal expansion of the membrane material [47]. In equation (28), $r_{p,0}$ is the pore size estimated at a reference temperature, T_0. α_{rp} is the temperature coefficient of the membrane pore size.

$$r_p = r_{p,0}[1 + \alpha_{rp}(T - T_0)] \quad (28)$$

This relationship does not lead to a linear dependency of the hydrodynamic membrane resistance with the temperature. Combined with the effects of the temperature on the viscosity and the diffusion rates, the flux through the membrane increases strongly with the temperature. Within a limited temperature range, the flux increase can still be approximated by a linear decrease in the hydrodynamic resistance (equation (29)).

$$R_m = R_{m,0}[1 + \alpha_{Rm}(T - T_0)] \quad (29)$$

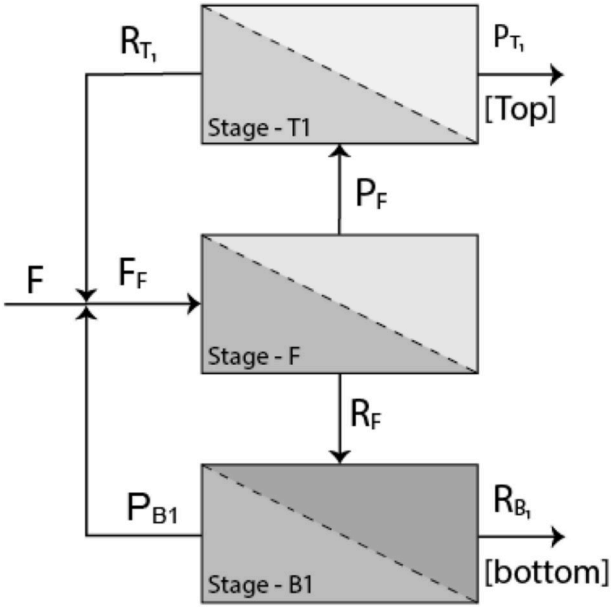

Fig. 4. Schematic drawing of a 3-stage membrane cascade configuration based on the ideal design proposed by Lightfoot [48].

2.6. Membrane cascade setup

A membrane cascade consists of multiple stages of membranes arranged consecutively. A consecutive stage produces a more refined or more concentrated outlet stream and may recycle other streams to the previous stage. This way, the purity and yield of a single-stage membrane process can be improved. A schematic drawing of a 3-stage membrane cascade based on the ideal design proposed by Lightfoot [48] is shown in Fig. 4.

Within a 3-stage design, the streams follow the mass balance relationship. The total and component mass balances for the whole system are expressed in equations (30) and (31). These equation relate the flow rates (Fl) and concentration (C_i) in any position of the design. Subscripts F, $T1$ and $B1$ indicate the stages that the stream comes from.

$$Fl_F = Fl_{P_{T1}} + Fl_{R_{B1}} \quad (30)$$

$$C_{f,i}\ Fl_F = C_{p,i}\ Fl_{P_{T1}} + C_{r,i}\ Fl_{R_{B1}} \quad (31)$$

At the mixing point, the streams follow the mass balances as expressed in equations (32) and (33). Equations (34) and (35) give the mass balances over the membrane stages. The permeate from the feed stage is also the feed for stage T1, and the retentate acts as the feed for stage B1.

$$Fl_{F_F} = Fl_F + Fl_{R_{T1}} + Fl_{P_{B1}} \quad (32)$$

$$C_{f,i}\ Fl_{F_F} = C_{f,i}\ Fl_F + C_{r,i}\ Fl_{R_{T1}} + C_{p,i}\ Fl_{P_{B1}} \quad (33)$$

$$Fl_{F_{stage}} = Fl_{P_{stage}} + Fl_{R_{stage}} \quad (34)$$

$$C_{f,i}\ Fl_{F_{stage}} = C_{p,i}\ Fl_{P_{stage}} + C_{r,i}\ Fl_{R_{stage}} \quad (35)$$

3. Materials and methods

3.1. Materials

All experiments were performed using Frutalose L85® provided by Sensus (Roosendaal, the Netherlands). Frutalose is a FOS syrup with 75% dry matter. In this research, we use 0.5 wt% of this syrup for characterization experiments and 5 wt% for validation experiments. All dilutions were with demineralized water.

Table 1
Feed concentration for characterization and validation experiments diluted in demineralized water.

Component	Concentration for characterization (g/L)[a]	Concentration for validation (g/L)[a]
Glucose	0.307 ± 0.019	3.126 ± 0.082
Fructose	0.073 ± 0.012	1.254 ± 0.030
DP2	0.396 ± 0.024	4.660 ± 0.120
DP3	0.706 ± 0.049	7.906 ± 0.196
DP4	0.769 ± 0.050	8.611 ± 0.214
DP ≥ 5	1.329 ± 0.089	14.973 ± 0.369

[a] Uncertainties are calculated based on the 95% confidence interval for all experiments.

Frutalose is a mixture of FOS with a DP ranging from 3 to 10, as well as mono- and disaccharides. In our study, oligosaccharides with a DP of 5 and higher are treated as one lumped component. We ascribe average physical properties to this lumped component, based on its overall weight fraction. The feed concentration of FOS solution used in this research is shown in Table 1.

3.2. Filtration experiment setup

All experiments were performed using a pilot-scale membrane unit with a process volume of 10 L. The experiments were divided into 2 groups: characterization experiments and validation experiments. The characterization experiments were performed to estimate the membrane resistance R_m and the pore size r_p using 0.5% FOS syrup diluted in demineralized water. The characterization experiments were performed at 5 temperatures between 25 °C and 45 °C with an interval of 5 °C, and using transmembrane pressures (TMP) between 4 and 16 bar. The model that was developed using the characterized membrane properties was then validated using 5% FOS syrup in demineralized water. These validation experiments were performed at 3 temperatures (25 °C, 35 °C, and 45 °C) and 3 TMPs (8, 12 and 16 bar).

We used 3 different membranes which vary in molecular weight cut-off: GE (MWCO 1kDa), GH (MWCO 2.5 kDa) and GK (MWCO 3.5 kDa). All membranes are model 1812C-34D from General Electric (GE Osmonics, Sterlitech, Kent, WA, USA) with an effective membrane area of 0.38 m^2. The validation experiments were performed later using these same membranes. All experiments were carried out using a crossflow velocity of 0.10 m/s until steady state conditions were reached. The steady state condition was indicated by a constant refractive index at both permeate and retentate streams, which were measured inline. In practice, this was reached within 25 min.

3.3. Analyses

The FOS samples were analysed for their concentrations at all DPs. Components with a DP higher than 5 were analysed as 1 lumped component. The analyses were performed using high-performance liquid chromatography. A Shodex column (KS-802 8.0 × 300 mm) integrated with a refractive index detector (Shodex RI-501) was used. The chromatography system was operated at 50 °C using deionized water (Milli-Q®) as eluent at a flow rate of 1 mL/min. The retention times of all FOS components in the chromatography system are presented in Table 2.

Table 2
Retention time of carbohydrate components in HPLC analysis.

Component	Retention time (min)[a]
Glucose	10.00 ± 0.15
Fructose	9.40 ± 0.10
DP2	8.40 ± 0.10
DP3	8.00 ± 0.15
DP4	7.50 ± 0.15
DP ≥ 5	7.20 ± 0.20

[a] The interval represents the window of detection for particular components.

3.4. Computational approach

The membrane resistance, R_m, was estimated using the experimental clean water flux. Using only water in the experiments eliminates the osmotic pressure effect in equation (14). The membrane resistance can then be calculated using the viscosity of water and establishing a linear regression between the TMP and the volumetric flux.

The membrane pore size, $r_{p,i}$, was estimated using very diluted FOS syrup (Table 1, second column). Under this condition, the effect of osmotic pressure in equation (14) was assumed to be small and thus negligible. The same assumption was made by Aguirre et al. [14] to characterize their membrane using a modified SPM. The pore size estimation was performed by minimizing the sum of the squared errors between the predicted and the experimental rejection values (equation (36)). The experimental solute rejection was calculated with equation (26) using the measured concentrations at the permeate and retentate. The predicted solute rejection was calculated using equation (23) by solving the other relations in Section 2.3. The fitting procedure to estimate $r_{p,i}$ was performed by minimizing the residual SR_R (with the *optimize* function in R [49]) as defined in equation (36).

$$SR_R = \left(R_{r,i_{experiment}} - R_{r,i_{predicted}}\right)^2 \tag{36}$$

We did not estimate the pore size distribution; instead, different pore sizes were estimated for every solute, membrane and temperature point as mentioned in Section 3.2.

The estimated membrane resistance and the pore size were then fitted in temperature-dependent models (equations (28) and (29)) to estimate the standard values ($r_{p,0}$ and $R_{m,0}$) and the temperature coefficients (α_{Rm} and α_{rp}) through linear regression. These linear regressions were computed using the *lm* function in R [49]. The same function was also used to estimate the parameters in quadratic models in equations (7) and (8) from literature data.

Using the standard values of the membrane resistance, pore size and their temperature coefficients, we can predict the outcome of a single-stage membrane. This model was validated using a higher concentration than the characterization experiments (Table 1, third column). In this case, the osmotic pressure was taken into account. To estimate the osmotic pressure, the permeate concentration is required, creating a circular calculation. In this study, we used the iterative approach developed by Yun and Petkovic [50] to solve this circular calculation. The model was then extended to predict the outcome of a cascaded system (Fig. 4) by solving the mass balances (equations (30)–(35)).

The separation performance for both single and cascaded membrane was evaluated according to the product purity and yield. For FOS, all oligosaccharides with DP higher than 3 are considered valuable. In a single-stage separation, the retentate stream was considered as being the most valuable product, whereas in a cascaded system, stream R_{B1} was considered to be the target product. Based on those considerations, equations (37) and (38) were formulated to describe the product purity and yield.

$$\text{Purity} = \frac{\sum_{i=3}^{5} C_{r,i}}{\sum_{i=1}^{5} C_{r,i}} \times 100\% \tag{37}$$

$$\text{Yield} = \frac{\sum_{i=3}^{5} C_{r,i}\ Fl_R}{\sum_{i=1}^{5} C_{r,i}\ Fl_F} \times 100\% \tag{38}$$

3.5. Viscosity analysis

To estimate the parameters in the temperature-dependent viscosity model (equation (13)), the viscosity of FOS at various concentrations and temperatures was measured using an Anton Paar MCR 502 rheometer (Graz, Austria) in a temperature range of 25°C-45 °C with a 5 °C interval. Dilutions of FOS syrup in demineralized water at concentrations of 1.5–8.5 wt% were used.

The parameters in equation (13) were estimates using a non-linear solver (*nls* function) in R [49]. This function minimized the square of residuals between the predicted and measured viscosity (equation (39)).

$$SR_{\eta} = \left(\eta_{measured} - \eta_{predicted}\right)^2 \tag{39}$$

4. Results and discussion

4.1. Viscosity model

Our extension of the model by Chirife and Buera [40], shown in equation (13), showed good agreement with experiments using FOS at various concentrations (mole fraction) as shown in Fig. 5. The fitted parameters were estimated and expressed in equation (39). In this equation, fitted parameter b^* is presented in J/g and c^* in J/ mol. Using this equation, the viscosity of oligosaccharide mixtures at any temperature and concentration can be predicted. In addition to the temperature effect, the ability to predict the viscosities at any concentration is also important for further application in a cascaded design. In a cascade system, each stage has different concentrations as the streams are getting more concentrated at the bottom stage and less concentrated at the top stage.

$$\frac{\eta_s}{\eta_w} = (1.043 \pm 0.011)\exp\left\{\frac{(228.2 \pm 24.91)\ \overline{MW} + (27{,}620 \pm 10{,}400)}{R_g T} X\right\} \tag{40}$$

4.2. Membrane resistance and flux prediction

In this section, we discuss the effect of the temperature on the membrane resistance and the flux in total, as a combination of both the viscosity and the membrane resistance. The resistance and the clean water flux are discussed first, and later extended to systems with solutes.

Fig. 6 confirms the linearity of the relationship between the temperature and the membrane resistance. The estimated parameters from Darcy's law are summarized in Table 3. Both the figure and the table show that the GH and GK membranes had a lower resistance at higher temperatures, while the GE membrane showed the opposite. The behaviour of the GH and GK membranes was expected, because the membrane material expands at higher temperatures, which also enlarges the pores. The opposite behaviour of the GE membrane might come from the fabrication of the membrane itself. Whereas the GH and GK were both polysulfone/polyamide composites, the GE membrane was a composite polyamide.

Fig. 6 also depicts that the estimated inaccuracies were much larger in the GE membrane, and they were smaller in the GH membrane and even smaller in the GK membrane. This could be related to measurement inaccuracies. The measured permeate flow rate was used to calculate the flux, which was later used to estimate the membrane resistance. The GE membrane exhibited low permeate flows, which resulted in larger inaccuracies than with the higher flow rates that were measured with the GH and GK membranes. Regardless, the inaccuracy in the temperature constant, α_{Rm}, did not show this relationship; all errors were in the same order of magnitude with the estimates. This may result from error propagation in the calculation.

Because both the viscosity and the membrane resistance depend on the temperature, the clean water flux through the membrane also depends on the temperature. Fig. 7 shows the temperature effect on the flux for 3 different membranes. All membranes showed strong increases in the clean water flux with temperature, despite the opposite behaviour of the membrane resistance of the GE membrane. The viscosity is therefore the dominant factor in the temperature dependence of the clean water flux for the GE membrane.

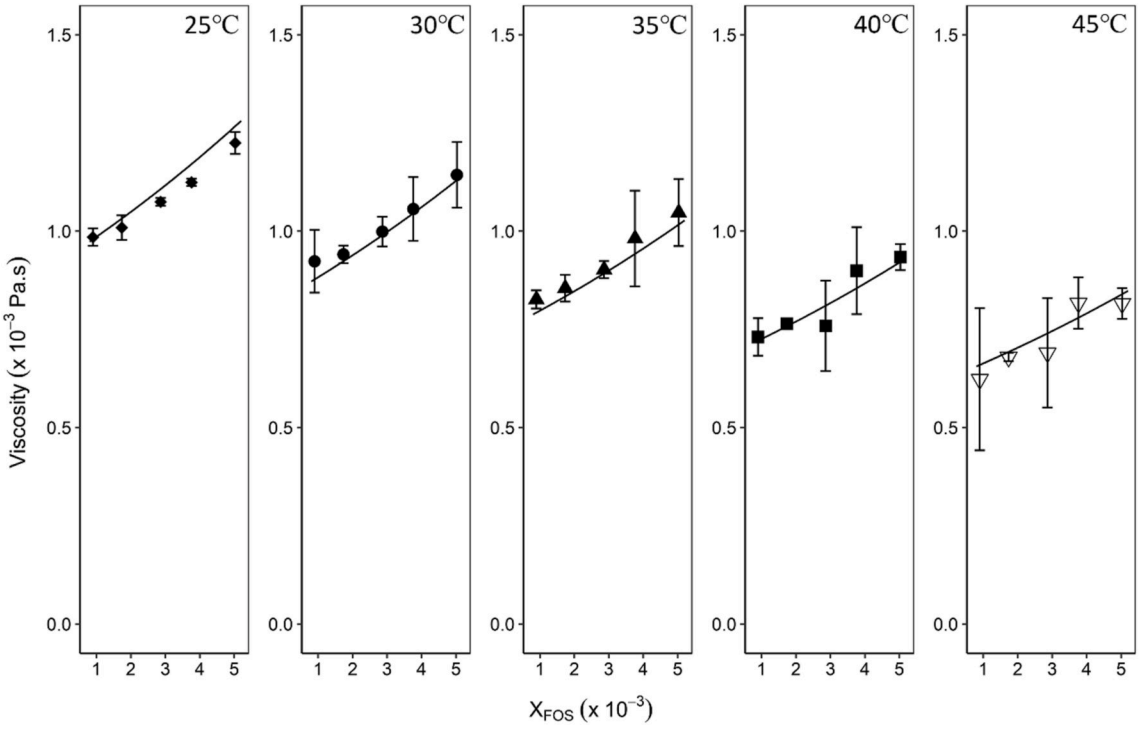

Fig. 5. Validation of the temperature-dependent viscosity model (equation (13)) using various FOS concentrations (as mole fractions) at a temperature range of 25°C-45 °C.

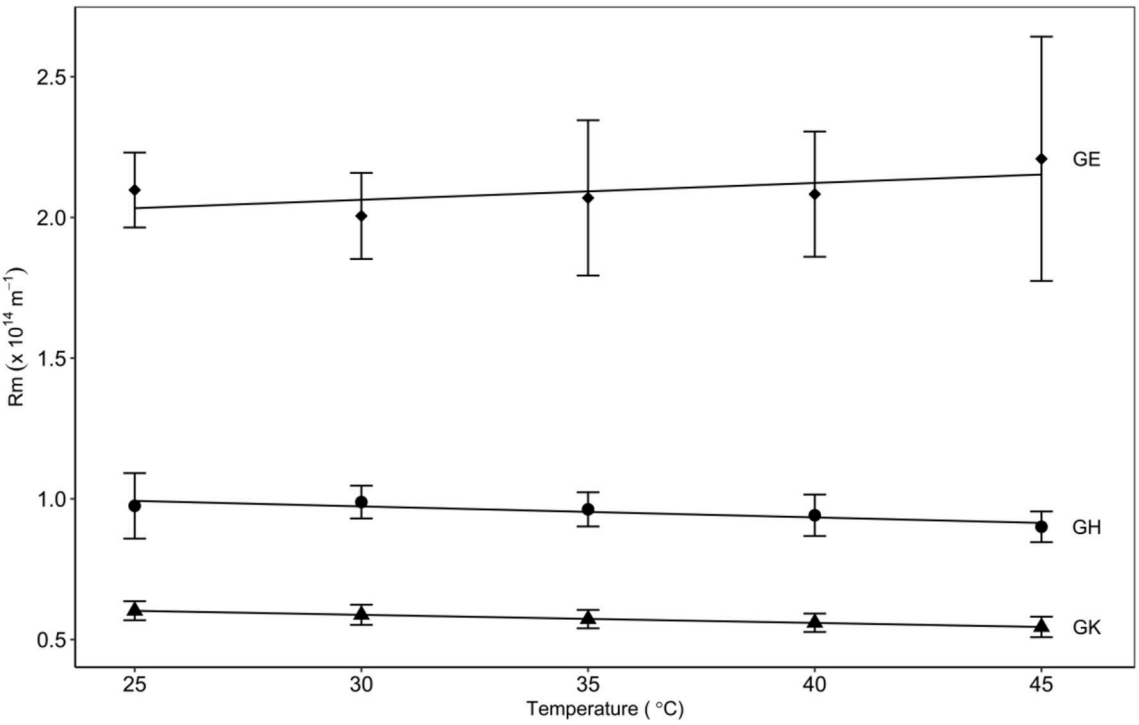

Fig. 6. Linear relationship between temperature and membrane resistance for 3 different membranes. Membrane resistances were estimated using clean water flux at various pressures.

Table 3
Estimated parameters for the temperature dependency model of membrane resistance (equation (34)).

Membrane	Rm_0 ($\times 10^{13}\ m^{-1}$)	α_{Rm} ($\times\ 10^{-3}\ m^{-1}K^{-1}$)
GE	20.33 ± 0.99	2.94 ± 3.98
GH	9.93 ± 0.79	−3.94 ± 6.53
GK	6.02 ± 0.27	−4.77 ± 3.68

The 3 membranes used in this study, being polymeric membranes, might show an irreversible response to heating, as commonly observed in many polymers as they cross their glass transition temperature (T_g). We observed a hysteresis upon immediate cooling in the GE membrane. The membrane resistance at lower temperatures showed higher values than its initial resistance after being operated at 45 °C, resulting in lower fluxes. This implied that the T_g for the GE membrane lies within 25°C-45 °C. Further detail about the glass transition was not studied in this research. However, from Fig. 6, we guess that this point existed between 30 °C and 35 °C for the GE membrane. The resistance initially decreased from 25 °C to 30 °C, as expected from the other membranes, and then increased from 30 °C to 45 °C. Membranes that operate above the glass transition temperature might experience a compaction resulting in a non-linear relationship between TMP and the flux. We indeed observed this behaviour in the GE membrane as shown inFig. 7.

This effect was only observed in the GE membrane upon immediate cooling. We did observe that the resistance of the GE membrane returned to its original value, as reported in Fig. 6, after storage. This implies that the membrane was able to slowly restructure during storage. For the other membranes, the resistance returned to its initial value upon immediate cooling after being operated at 45 °C. This better explained the linear relationships for both temperature–resistance and TMP–flux for GH and GK membranes.

4.3. Temperature effect on membrane pore size

The membrane pore size was estimated by fitting the pore size to the data using the modified SPM (Section 2.3). Fig. 8 shows the rejections from the fitted model and the experimental data at 45 °C. The same estimation procedure was repeated for every temperature point in duplicate; figures similar to Fig. 8 can be constructed for every repetition (see supplementary material). Using the estimates at all repetitions, a linear relationship between the pore size and the temperature was then determined by estimating the standard pore size, $r_{p,i,0}$, and the temperature coefficient, α_{rp}.

This was done for every solute, resulting in 5 values of pore sizes corresponding to 5 solutes. These values could be compiled into a mean pore size and a standard distribution, as explained in the work of Kuhn et al. [3]. However, in this work, we directly used the different pore size values that correspond to the 5 solutes. The translation towards a normal distribution would not have added predictive value to the model, and the direct use avoids the assumption of having a normal pore size distribution, which is an approximation at best.

Fig. 9 shows linear relationships between the temperature and the membrane pore sizes for DP4. Other solutes give similar relations (see supplementary material), which are summarized for the pore size $r_{p,i,0}$ and temperature increment α_{rp} in Table 4. Using both $r_{p,i,0}$ and α_{rp} values, the pore sizes at any temperature can be calculated using equation (28). The estimated pore sizes are in the range of those commonly reported for nanofiltration membranes (0.7–2 nm). The pore sizes for the GK membrane were the largest while the GH membrane had a similar pore size compared with the GE membrane. However, it was not clear what the operating temperature was for these specifications, which might have been higher than 25 °C; despite the similar pore size at 25 °C, the GH membrane had a higher temperature increment of the pore size. Therefore, the pore size of this membrane could be higher and different from that of a GE membrane at higher temperatures.

In addition, for all solutes, we observed larger temperature increments with a GK membrane compared with the other membranes, as shown in Fig. 9 and Table 4. The difference in these properties for

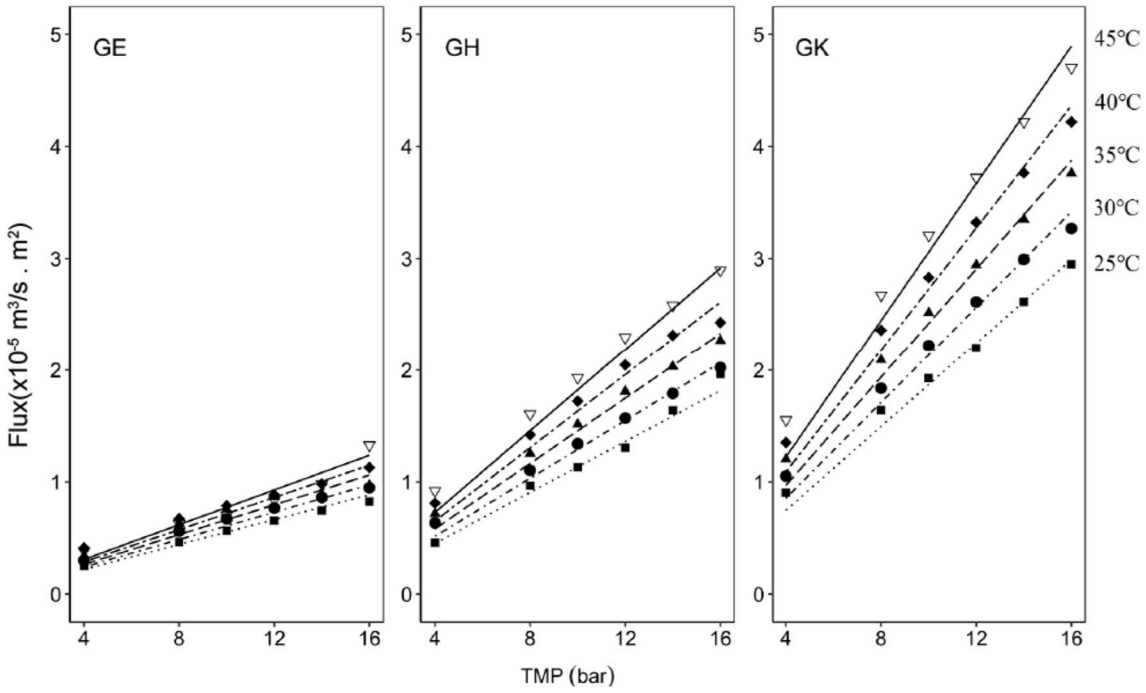

Fig. 7. Temperature effect of clean water flux for 3 different membranes.

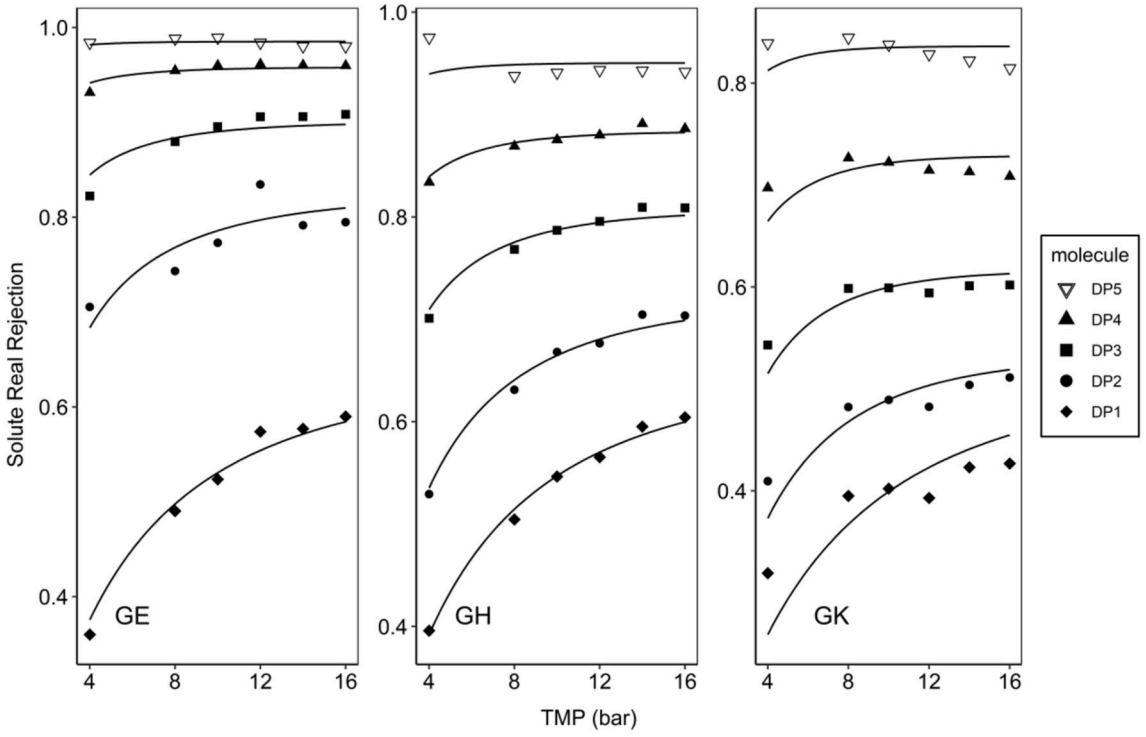

Fig. 8. The real rejection as function of pressure for 3 different membranes at 45 °C using 0.5% FOS syrup. The symbols represent the experiments. The lines are the fitted models with the estimated pore sizes.

different membranes might relate to the different materials and structure of the membrane.

Table 4 tells us that the thermal increments of the pore sizes (α_{rp}) over the temperature range considered were far lower than the absolute pore size ($r_{p,i,0}$). These values varied by a maximum of 2% for GK membrane. That gave us an increase of a maximum of 0.4 nm with a temperature increase of 20 °C, as used in this study.

As the temperature increases, both the solute and the membrane expand. Both changes affect the solute rejection. According to the modified SPM, the solute rejection was dependent on the solute to pore size ratio. When both change, a change in rejection would occur depending on the sizes of the 2 changes. Here, we report that the temperature expansions of the pore size and the hydrated volume of sugar are in the same order of magnitude. Despite the similar orders of

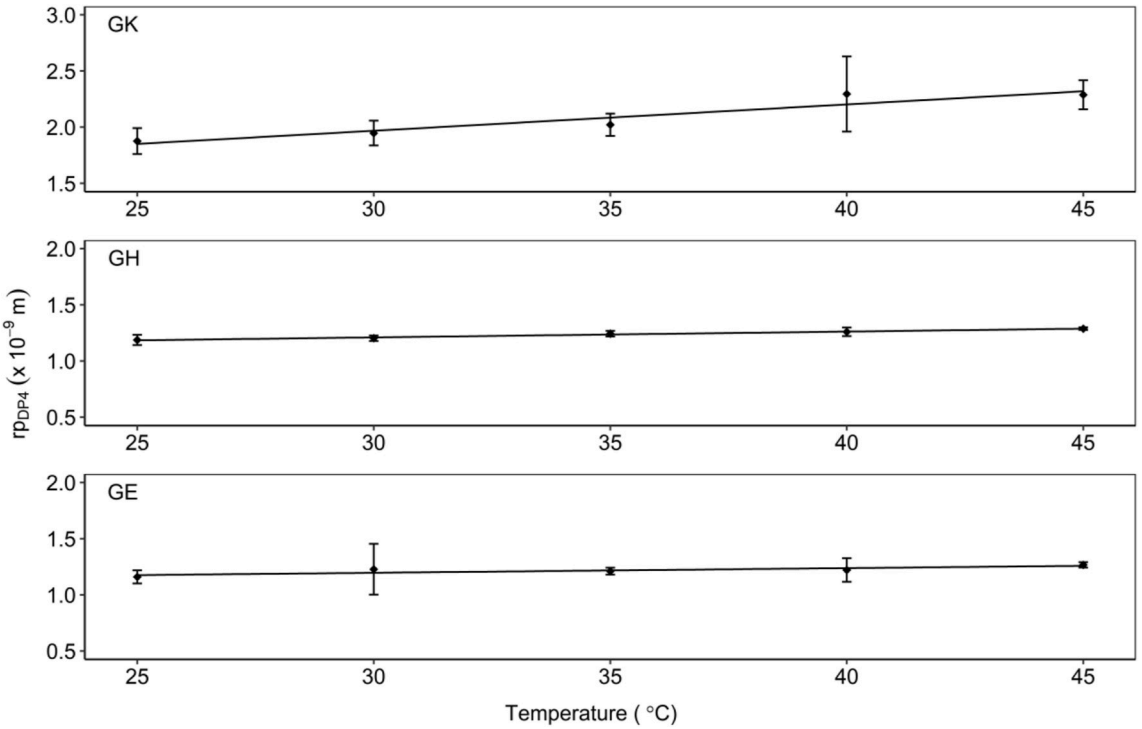

Fig. 9. Linear relationship of temperature and pore size corresponding to DP4 for different membranes.

Table 4
Estimate parameters (standard pore size and thermal increment) for the temperature dependency model of pore size with respect to each solute.

Membrane	Solute	$r_{G,i}$ ($\times 10^{-9}$ m) at 25 °C	$r_{p,i,0}$ ($\times 10^{-9}$ m)	α_{rp} ($\times 10^{-10}$ m/K)
GE	DP1	0.407	0.746 ± 0.014	0.011 ± 0.016
	DP2	0.601	0.950 ± 0.015	0.039 ± 0.013
	DP3	0.794	1.070 ± 0.016	0.045 ± 0.013
	DP4	0.987	1.176 ± 0.018	0.035 ± 0.013
	DP ≥ 5	1.330	1.461 ± 0.015	0.023 ± 0.009
GH	DP1	0.407	0.703 ± 0.007	0.013 ± 0.008
	DP2	0.601	0.921 ± 0.004	0.059 ± 0.004
	DP3	0.794	1.058 ± 0.006	0.054 ± 0.004
	DP4	0.987	1.184 ± 0.005	0.044 ± 0.003
	DP ≥ 5	1.330	1.486 ± 0.006	0.026 ± 0.003
GK	DP1	0.407	0.948 ± 0.062	0.070 ± 0.054
	DP2	0.601	1.598 ± 0.151	0.195 ± 0.079
	DP3	0.794	1.783 ± 0.096	0.168 ± 0.045
	DP4	0.987	1.851 ± 0.054	0.127 ± 0.024
	DP ≥ 5	1.330	2.101 ± 0.024	0.089 ± 0.009

magnitude, higher values were observed for the solute dimension, which results in a small increase in the solute to pore size ratio. Thus, we predict a small increase in the rejection.

4.4. Prediction of single-stage separations

With all parameters estimated using low concentrations, we can now predict the single-stage performance at realistic concentrations.

At higher solute concentrations, the concentration polarization effect is more prominent. This leads to a larger osmotic pressure difference over the membrane and hence a lower effective driving force. At the same time, the larger concentration of solutes at the membrane also implies more transmission of the solutes through the membrane and hence a lower effective rejection than the real rejection would indicate. The concentration polarization depends on the transmembrane flux, which depends on the membrane resistance and on the viscosity. In general, the membrane resistance decreases with temperature, and the solution viscosity decreases strongly. This together leads to a strong increase in the transmembrane flux with temperature.

The strong increase in the water flux with temperature is not followed by the solute flux. Even though the membrane expands with temperature, the solute itself also expands. This limits the solute transport, resulting in only a slight increase in the solute flux. A rapid increase in the water flux that is not followed by the solute flux results in only a slight increase in the solute rejection. Fig. 10 shows that the product purity indeed increases slightly with temperature. This was expected because the solute rejection only increased slightly. Among the 3 membranes, the GK membrane was the most sensitive to temperature change, because it had the highest temperature coefficient. Therefore, a higher FOS purity was obtained at higher temperatures.

The increase in flux at higher temperature resulted in a declining yield. As the temperature increases, the transmembrane flux increases strongly, and therefore, more of the feed ends up as permeate. As a consequence, less liquid is obtained as retentate. Most of the product stayed at the retentate side, but as the rejection was not 100%, a part of it also ended up in the permeate. Hence, if the permeate forms a larger part of the total volume, more of the product is lost into the permeate and hence the yield is lower. At the same time, producing more permeate also means that more of the "impurities" (smaller DPs) end up in the permeate. This effect was stronger for the smaller DPs than for the ≥ DP5 product, because their rejections were smaller, and the purity was

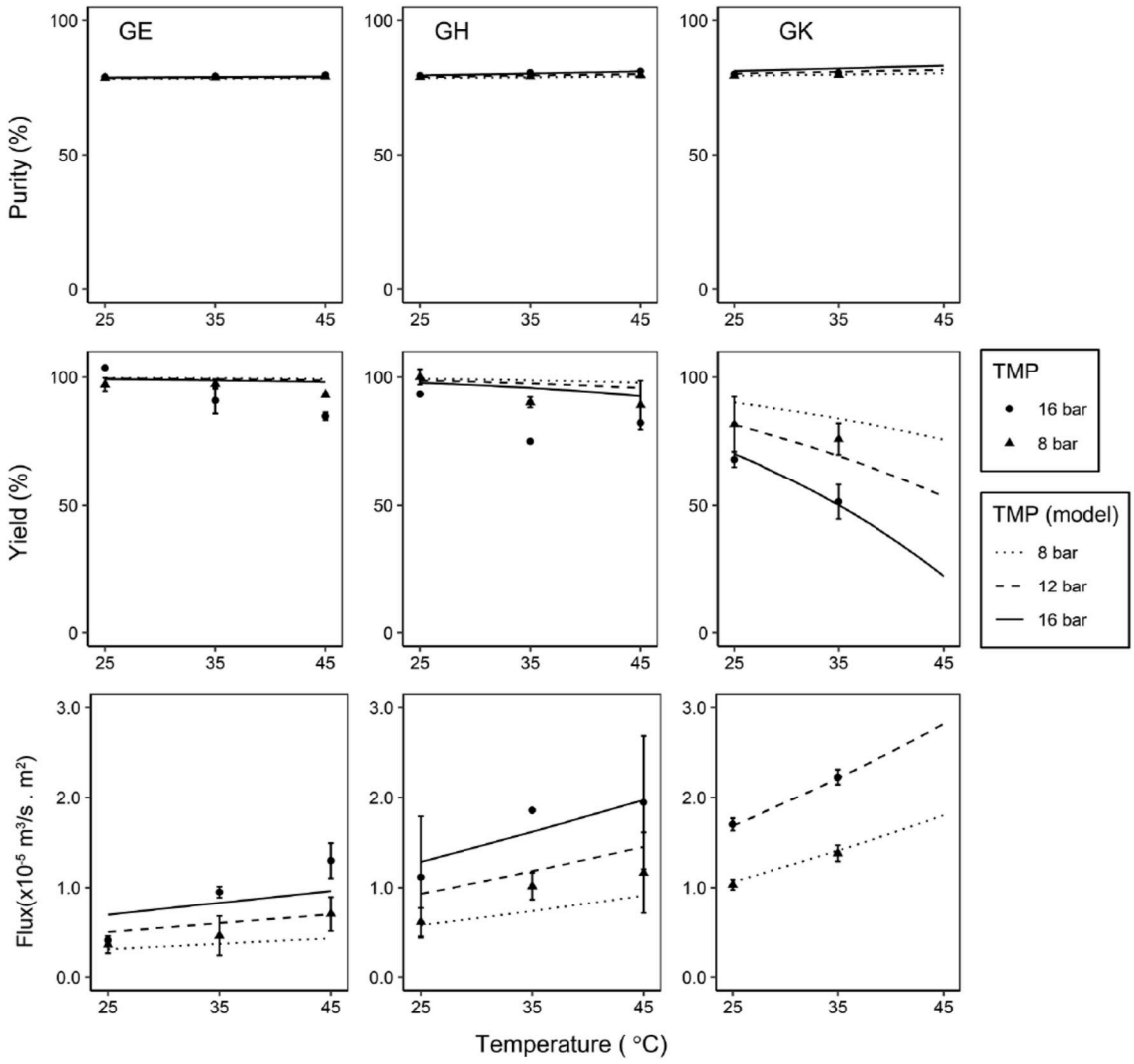

Fig. 10. Prediction of the temperature effect on the performance of single-stage membranes validated with 5% FOS syrup (experimentally) using a feed flow rate of 50 kg/h. The discontinued line for the GK membrane at 16 bar was due to insufficient flow rate at the retentate.

therefore slightly increased. The strongest decline in yield was observed with the GK membrane because it exhibited the largest flux increase with temperature (Section 4.2).

Fig. 10 shows a classic trade-off between purity and yield, but this trade-off was not the same for every membrane. In addition, the temperature effect in the product yield is strong. Based on these phenomena, we conclude that we can improve the separation performance by decreasing the temperature, resulting in a higher yield without losing product purity; however, this is at the cost of a lower throughput.

4.5. Performance of a 3-stage filtration cascade

The predictive model that was validated for single-stage membranes was extended to a cascaded system (Fig. 4). We selected 1 combination of process parameters as a standard, which was chosen based on the work of Aguirre et al. [29]. A membrane with double area at the feed stage was chosen. To achieve this in practice, two GK membranes were used at the feed stage and operated at a TMP of 8 bar. After the feed stage, a GH membrane was used at the top stage using a TMP of 16 bar and a GK membrane operated at a TMP of 12 bar at the bottom. The feed stream entered the feed stage at 50 kg/h.

One of the advantages of using a cascade is that each stage can be run at a different temperature. To simplify the investigation, we simulated the separation process for 2 scenarios: a homogeneous and an inhomogeneous temperature configuration. In the homogeneous configuration, the temperature was equal at all stages and was varied as a whole. In the inhomogeneous configuration, the temperature at 1 stage differed from the others. Here, 3 different cases were assessed: the feed, top and bottom cases. In these cases, the temperature in 1 stage was varied from 25 °C to 45 °C, and the temperatures of the other stages were constant at 45 °C.

Fig. 11 shows the effect of the temperature on the purities and yields obtained with the membrane cascade as a function of the temperature, with the homogeneous (a) and inhomogeneous (b) temperature configurations. For all systems, qualitatively similar behaviour as in a single-stage separation was observed. The yield could be increased by lowering the temperature while the purity remained essentially the same (around 80%). The purity achieved using a cascade system (see Fig. 11) was higher than using a single-stage separation (see Fig. 10), which of course was the main purpose of using a cascaded system.

In an inhomogeneous configuration, the temperature effect on the product yield varies depending on which stage is varied in temperature. The effect of temperature was more substantial for the top stage, whereas it had hardly any effect at the bottom stage. This was related to the destination of the permeate flow at each stage. The permeate of the bottom stage was recycled to the feed stage, and the permeate of the feed

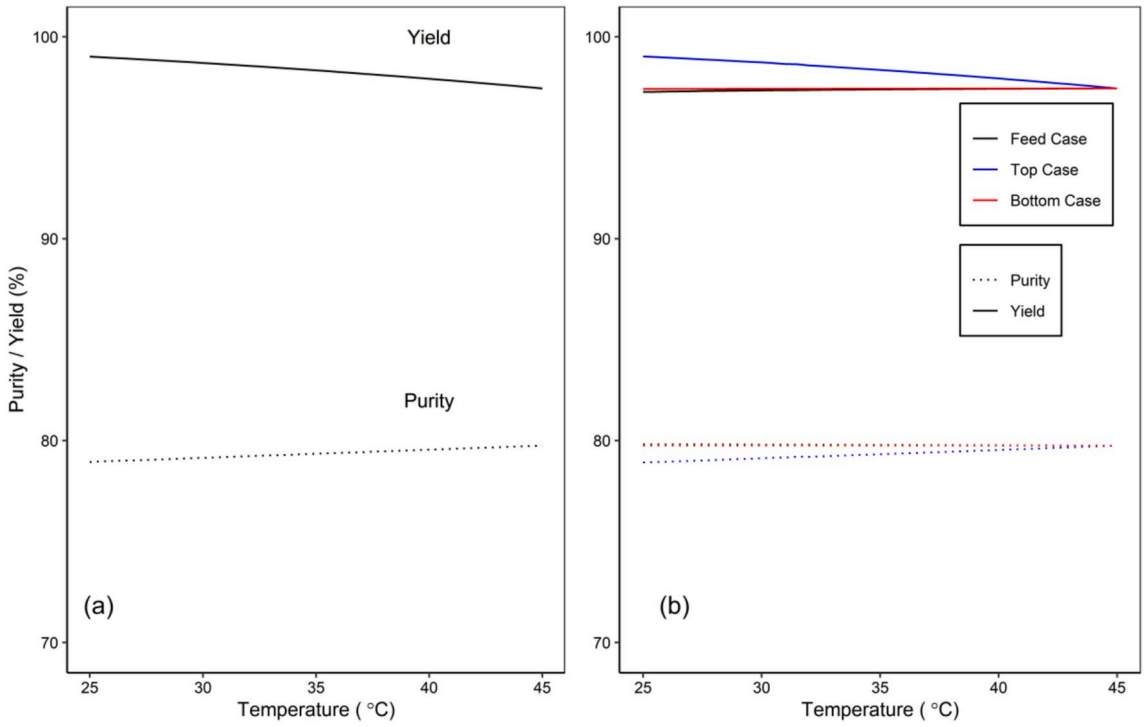

Fig. 11. Temperature effect in the cascaded filtration system using the homogeneous (a) and inhomogeneous (b) temperature setup. In the inhomogeneous setup, the temperature at 2 other stages were set at 45 °C, and 1 was varied according to the case. All simulations were done using a feed flow rate of 50 kg/h.

stage forms the feed of the top stage. Therefore, the permeate streams of these 2 stages were processed again. On the other hand, the permeate of the top stage was directly extracted from the system. In the case of FOS ($\geq$ DP3), the oligosaccharides in the permeate of the top stage are considered as a loss, lowering the yield of the oligosaccharides in the bottom retentate. Although the purity of the stream remained more or less the same, the increase in the permeate flow rate at the top stage directly reduced the yield. Using this treatment, the separation can achieve 97% yield.

5. Conclusions

The effect of the temperature on the nanofiltration of a mixture of fructo-oligosaccharides was investigated through experiment and through modelling. An increase in the temperature affects the process in 3 ways: (1) it expands the solute, (2) it reduces the solution viscosity, and (3) it expands the membrane pore size while at the same time reducing its hydraulic resistance. All these factors contribute to the overall performance of a filtration process, which was assessed by measuring and modelling its purity and yield.

Although the fluxes become much larger with increasing temperature, the temperature hardly affects the product rejection and purity. However, the yield is strongly affected by the temperature, with higher yields at lower temperatures. This is related to the larger fluxes at higher temperature, leading to a larger split of the feed into the permeate, and more of the product ending up in the permeate flow. Similar behaviour was observed in a 3-stage cascaded system. The temperature effect was more prominent at the top stage, due to the permeate stream that is directly extracted off the system.

Authors and contributions

Zulhaj Rizki: conceptualization, methodology, software, validation, formal analysis, investigation, writing - original draft, writing – review and editing and visualization.

Eric Suryawirawan: validation, formal analysis, writing – review and editing.

Anja E.M. Janssen: conceptualization, writing – review and editing and supervision.

Remko M. Boom: conceptualization, writing – review and editing and supervision.

Albert van der Padt: conceptualization, writing – review and editing and supervision.

Declaration of competing interest

The authors declare that they have no known competing financial interests or personal relationships that could have appeared to influence the work reported in this paper.

Acknowledgements

The authors would like to acknowledge Lembaga Pengelola Dana Pendidikan (LPDP), and Kementrian Keuangan Indonesia for financial support.

Appendix A. Supplementary data

Supplementary data to this article can be found online at https://doi.org/10.1016/j.memsci.2020.118292.

Nomenclature

C	solute concentration [g L^{-1}]
D	diffusion coefficient [m^2 s^{-1}]
d_h	hydraulic diameter [m]
D_p	diffusion coefficient inside the pore [m^2 s^{-1}]
E	dimensionless parameter in the viscosity model [dimensionless]
Fl	flow rate [kg h^{-1}]
J_v	volumetric flux [m^3 s^{-1} m^{-2}]
k	mass transfer coefficient [m s^{-1}]
k^*	corrected mass transfer coefficient [m s^{-1}]
k_B	Boltzmann constant [1.38×10^{-23} m^2 kg s^{-2} K^{-1}]
K_c	convective hindrance coefficient [dimensionless]
K_D	diffusive hindrance coefficient [dimensionless]
K_Y	lumped parameter in the modified SPM [dimensionless]
L_0	capsule diameter [m]
L_1	capsule length [m]
MW	molecular weight [kg mol^{-1}]
n_h	hydration number [dimensionless]
P	product purity [wt%]
Pe	Peclet number [dimensionless]
R_g	gas constant [J mol^{-1} K^{-1}]
r_G	Giddings radius [m]
R_m	membrane resistance [m^{-1}]
r_p	pore radius [m]
R_r	real rejection coefficient [dimensionless]
r_S	Stokes radius [m]
T	process temperature [K]
T_0	reference temperature [25 °C]
TMP	transmembrane pressure [Pa]
u	crossflow velocity [m s^{-1}]
V	solvent velocity [m s^{-1}]
$V_{m,b}$	bare molar volume of non-hydrated components [m^3]
$V_{m,bw}$	molar volume of bound water [m^3]
$V_{m,h}$	molar volume of hydrated components [m^3]
X	total sugar molar fraction [dimensionless]
Y	product yield [%]

Greek letters

α_{Rm}	temperature coefficient for membrane resistance [K^{-1}]
α_{rp}	temperature coefficient for membrane pore radius [K^{-1}]
η_s	solution viscosity [Pa s]
η_w	water viscosity [Pa s]
λ	solute to pore ratio [dimensionless]
π_o	osmotic pressure [Pa]
ρ	density [kg m^{-3}]
φ	partition coefficient [dimensionless]

Subscripts

F, $T1$, $B1$	stage
i	solute, degree of polymerization
m	membrane wall
p	permeate side
P, R	permeate and retentate streams
r	retentate side

References

[1] A. Zydney, Protein separations using membrane filtration: new opportunities for whey fractionation, Int. Dairy J. 8 (1998) 243.

[2] Y.M. Feng, X.L. Chang, W.H. Wang, R.Y. Ma, Separation of galacto-oligosaccharides mixture by nanofiltration, J. Taiwan Inst. Chem. Eng. 40 (2009) 326–332, https://doi.org/10.1016/j.jtice.2008.12.003.

[3] R.C. Kuhn, F. Maugeri Filho, V. Silva, L. Palacio, A. Hernández, P. Prádanos, Mass transfer and transport during purification of fructooligosaccharides by nanofiltration, J. Membr. Sci. 365 (2010) 356–365, https://doi.org/10.1016/j.memsci.2010.09.031.

[4] A.K. Goulas, P.G. Kapasakalidis, H.R. Sinclair, R.A. Rastall, A.S. Grandison, Purification of oligosaccharides by nanofiltration, J. Membr. Sci. 209 (2002) 321–335, https://doi.org/10.1016/S0376-7388(02)00362-9.

[5] M. Minhalma, L.L. Beal, I. Catarino, M. Mateus, M.N. de Pinho, Optimization of saccharide fractionation using nanofiltration/ultrafiltration, Desalination 199 (2006) 337–339, https://doi.org/10.1016/j.desal.2006.03.079.

[6] J. Hiddink, R. de Boer, P.F.C. Nooy, Reverse osmosis of dairy liquids, J. Dairy Sci. 63 (1980) 204–214, https://doi.org/10.3168/JDS.S0022-0302(80)82915-8.

[7] B. Van der Bruggen, M. Mänttäri, M. Nyström, Drawbacks of applying nanofiltration and how to avoid them: a review, Separ. Purif. Technol. 63 (2008) 251–263, https://doi.org/10.1016/j.seppur.2008.05.010.
[8] J. Marriott, E. Sørensen, A general approach to modelling membrane modules, Chem. Eng. Sci. 58 (2003) 4975–4990, https://doi.org/10.1016/J.CES.2003.07.005.
[9] J. Marriott, E. Sørensen, I.D. Bogle, Detailed mathematical modelling of membrane modules, Comput. Chem. Eng. 25 (2001) 693–700, https://doi.org/10.1016/S0098-1354(01)00670-6.
[10] W.R. Bowen, A.W. Mohammad, N. Hilal, Characterisation of nanofiltration membranes for predictive purposes — use of salts, uncharged solutes and atomic force microscopy, J. Membr. Sci. 126 (1997) 91–105, https://doi.org/10.1016/S0376-7388(96)00276-1.
[11] J.E. Almazán, E.M. Romero-Dondiz, V.B. Rajal, E.F. Castro-Vidaurre, Nanofiltration of glucose: analysis of parameters and membrane characterization, Chem. Eng. Res. Des. 94 (2015) 485–493, https://doi.org/10.1016/J.CHERD.2014.09.005.
[12] N.S. Kotrappanavar, A.A. Hussain, M.E.E. Abashar, I.S. Al-Mutaz, T. M. Aminabhavi, M.N. Nadagouda, Prediction of physical properties of nanofiltration membranes for neutral and charged solutes, Desalination 280 (2011) 174–182, https://doi.org/10.1016/J.DESAL.2011.07.007.
[13] A.W. Mohammad, A modified Donnan-steric-pore model for predicting flux and rejection of dye/NaCl mixture in nanofiltration membranes, Separ. Sci. Technol. 37 (2002) 1009–1029, https://doi.org/10.1081/SS-120002238.
[14] V. Aguirre Montesdeoca, J. Bakker, R.M. Boom, A.E.M. Janssen, A. Van der Padt, Ultrafiltration of non-spherical molecules, J. Membr. Sci. 570–571 (2019) 322–332, https://doi.org/10.1016/j.memsci.2018.10.053.
[15] A.A. Hussain, M.E.E. Abashar, I.S. Al-Mutaz, Effect of ion sizes on separation characteristics of nanofiltration membrane systems, J. King Saud Univ. Eng. Sci. 19 (2006) 1–18, https://doi.org/10.1016/S1018-3639(18)30844-4.
[16] S. Bandini, V. Morelli, Effect of temperature, pH and composition on nanofiltration of mono/disaccharides: experiments and modeling assessment, J. Membr. Sci. 533 (2017) 57–74, https://doi.org/10.1016/j.memsci.2017.03.021.
[17] M.L. Stewart, D.A. Timm, J.L. Slavin, Fructooligosaccharides exhibit more rapid fermentation than long-chain inulin in an in vitro fermentation system, Nutr. Res. 28 (2008) 329–334, https://doi.org/10.1016/j.nutres.2008.02.014.
[18] J.R. Hess, A.M. Birkett, W. Thomas, J.L. Slavin, Effects of short-chain fructooligosaccharides on satiety responses in healthy men and women, Appetite 56 (2011) 128–134, https://doi.org/10.1016/j.appet.2010.12.005.
[19] G. Flamm, W. Glinsmann, D. Kritchevsky, L. Prosky, M. Roberfroid, Inulin and oligofructose as dietary fiber: a review of the evidence, Crit. Rev. Food Sci. Nutr. 41 (2001) 353–362, https://doi.org/10.1080/20014091091841.
[20] K.R. Niness, Nutritional and health benefits of inulin and oligofructose, inulin and oligofructose: what are they? J. Nutr. (1999) 1431–1433.
[21] D. Meyer, S. Bayarri, A. Tárrega, E. Costell, Inulin as texture modifier in dairy products, Food Hydrocolloids 25 (2011) 1881–1890, https://doi.org/10.1016/j.foodhyd.2011.04.012.
[22] A. Tárrega, J.D. Torres, E. Costell, Influence of the chain-length distribution of inulin on the rheology and microstructure of prebiotic dairy desserts, J. Food Eng. 104 (2011) 356–363, https://doi.org/10.1016/j.jfoodeng.2010.12.028.
[23] B. Villegas, I. Carbonell, E. Costell, Inulin milk beverages: sensory differences in thickness and creaminess using R-index analysis of the ranking data, J. Sensory Stud. 22 (2007) 377–393, https://doi.org/10.1111/j.1745-459X.2007.00111.x.
[24] M.T.C. Machado, S. Trevisan, J.D.R. Pimentel-Souza, G.M. Pastore, M.D. Hubinger, Clarification and concentration of oligosaccharides from artichoke extract by a sequential process with microfiltration and nanofiltration membranes, J. Food Eng. 180 (2016) 120–128, https://doi.org/10.1016/j.jfoodeng.2016.02.018.
[25] W. Li, J. Li, T. Chen, C. Chen, Study on nanofiltration for purifying fructo-oligosaccharides I. Operation modes, J. Membr. Sci. 245 (2004) 123–129, https://doi.org/10.1016/j.memsci.2004.07.021.
[26] V. Aguirre Montesdeoca, A.E.M. Janssen, R.M. Boom, A. Van der Padt, Fine ultrafiltration of concentrated oligosaccharide solutions – hydration and pore size distribution effects, J. Membr. Sci. (2019), https://doi.org/10.1016/j.memsci.2019.03.019.
[27] A. Córdova, C. Astudillo, L. Santibañez, A. Cassano, R. Ruby-Figueroa, A. Illanes, Purification of galacto-oligosaccharides (GOS) by three-stage serial nanofiltration units under critical transmembrane pressure conditions, Chem. Eng. Res. Des. 117 (2017) 488–499, https://doi.org/10.1016/j.cherd.2016.11.006.
[28] N.V. Patil, T. Schotel, C.V. Rodriguez Gomez, V. Aguirre Montesdeoca, J.J. Sewalt, A.E. Janssen, R.M. Boom, Continuous purification of galacto-oligosaccharide mixtures by using cascaded membrane filtration, J. Chem. Technol. Biotechnol. 91 (2016) 1478–1484, https://doi.org/10.1002/jctb.4746.
[29] V. Aguirre Montesdeoca, A. Van der Padt, R.M. Boom, A.E.M. Janssen, Modelling of membrane cascades for the purification of oligosaccharides, J. Membr. Sci. 520 (2016) 712–722, https://doi.org/10.1016/j.memsci.2016.08.031.
[30] Z. Rizki, A.E.M. Janssen, R.M. Boom, A. van der Padt, Oligosaccharides fractionation cascades with 3 outlet streams, Separ. Purif. Technol. 221 (2019) 183–194, https://doi.org/10.1016/J.SEPPUR.2019.03.086.
[31] R. Sharma, S. Chellam, Temperature effects on the transport of water, uncharged and charged solutes across polymeric nanofiltration membranes, Am. Water Work. Assoc. Membr. Technol. Conf. (2007) 17–20, https://doi.org/10.1016/j.scitotenv.2011.11.081.
[32] T. Tsuru, S. Izumi, T. Yoshioka, M. Asaeda, Temperature effect on transport performance by inorganic nanofiltration membranes, AIChE J. 46 (2000) 565–574, https://doi.org/10.1002/aic.690460315.
[33] N.V. Patil, X. Feng, J.J.W. Sewalt, R.M. Boom, A.E.M. Janssen, Separation of an inulin mixture using cascaded nanofiltration, Separ. Purif. Technol. 146 (2015) 261–267, https://doi.org/10.1016/j.seppur.2015.03.061.
[34] Z. Rizki, A.E.M. Janssen, G.D.H. Claassen, R.M. Boom, A. van der Padt, Multi-criteria design of membrane cascades: selection of configurations and process parameters, Separ. Purif. Technol. 237 (2020) 116349, https://doi.org/10.1016/j.seppur.2019.116349.
[35] Y. Sano, S. Yamamoto, Mutual diffusion coefficient of aqueous sugar solutions, J. Chem. Eng. Jpn. 26 (1993) 633–636, https://doi.org/10.1252/jcej.26.633.
[36] J.C. Giddings, E. Kucera, C.P. Russell, M.N. Myers, Statistical theory for the equilibrium distribution of rigid molecules in inert porous networks. Exclusion chromatography, J. Phys. Chem. 72 (1968) 4397–4408, https://doi.org/10.1021/j100859a008.
[37] A. Gharsallaoui, B. Rogé, J. Génotelle, M. Mathlouthi, Relationships between hydration number, water activity and density of aqueous sugar solutions, Food Chem. 106 (2008) 1443–1453, https://doi.org/10.1016/j.foodchem.2007.02.047.
[38] A.F. Fucaloro, Y. Pu, K. Cha, A. Williams, K. Conrad, Partial molar volumes and refractions of aqueous solutions of fructose, glucose, mannose, and sucrose at 15.00, 20.00, and 25.00°C, J. Solut. Chem. 36 (2007) 61–80, https://doi.org/10.1007/s10953-006-9100-7.
[39] H. Shiio, Ultrasonic interferometer measurements of the amount of bound water. Saccharides, J. Am. Chem. Soc. 80 (1958) 70–73, https://doi.org/10.1021/ja01534a020.
[40] J. Chirife, M.P. Buera, A simple model for predicting the viscosity of sugar and oligosaccharide solutions, J. Food Eng. 33 (1997) 221–226, https://doi.org/10.1016/S0260-8774(97)00060-5.
[41] J. Chirife, G. Favetto, C.F. Fontán, Microbial growth at reduced water activities: some physicochemical properties of compatible solutes, J. Appl. Bacteriol. 56 (1984) 259–268, https://doi.org/10.1111/j.1365-2672.1984.tb01346.x.
[42] G. Schock, A. Miquel, Mass transfer and pressure loss in spiral wound modules, Desalination 64 (1987) 339–352, https://doi.org/10.1016/0011-9164(87)90107-X.
[43] R. Bird, W. Stewart, E. Lightfoot, Transport Phenomena, John Wiley, New York, 1961.
[44] W.R. Bowen, J.S. Welfoot, Modelling of membrane nanofiltration-pore size distribution effects, Chem. Eng. Sci. 57 (2002) 1393–1407, https://doi.org/10.1016/S0009-2509(01)00412-2.
[45] W.R. Bowen, J.S. Welfoot, Modelling the performance of membrane nanofiltration-critical assessment and model development, Chem. Eng. Sci. 57 (2002) 1121–1137, https://doi.org/10.1016/S0009-2509(01)00413-4.
[46] P. Dechadilok, W.M. Deen, Hindrance factors for diffusion and convection in pores, Ind. Eng. Chem. Res. 45 (2006) 6953–6959, https://doi.org/10.1021/ie051387n.
[47] R.A. Serway, J.W. Jewett, Physics for Scientists and Engineers, with Modern Physics, ninth ed., Brooks/Cole, Boston, 2014.
[48] E.N. Lightfoot, T.W. Root, J.L. O'Dell, Emergence of ideal membrane cascades for downstream processing, Biotechnol. Prog. 24 (2008) 599–605, https://doi.org/10.1021/bp070335l.
[49] R.C. Team, R: a language and environment for statistical computing. https://www.r-project.org/, 2019.
[50] B.I. Yun, M.S. Petković, A quadratically convergent iterative method for nonlinear equations, J. Kor. Math. Soc. 48 (2011) 487–497, https://doi.org/10.4134/JKMS.2011.48.3.487.